Solid-State ^{17}O Magic-Angle and Dynamic-Angle Spinning NMR Study of the SiO_2 Polymorph Coesite

P. J. Grandinetti*

Department of Chemistry, The Ohio State University, 120 W. 18th Avenue, Columbus, Ohio 43210-1173

J. H. Baltisberger

Department of Chemistry, CPO 86, Berea College, Berea, Kentucky 40404

I. Farnan† and J. F. Stebbins

Department of Geological and Environmental Sciences, Stanford University, Stanford, California 94305

U. Werner‡ and A. Pines

Materials Sciences Division, Lawrence Berkeley Laboratory and Department of Chemistry, University of California, Berkeley, California 94720

Received: January 6, 1995; In Final Form: March 21, 1995®

Five distinctly resolved ^{17}O solid-state NMR resonances in room temperature coesite, an SiO_2 polymorph, have been observed and assigned using dynamic-angle spinning (DAS) at 11.7 T along with magic-angle spinning (MAS) spectra at 9.4 and 11.7 T. The ^{17}O quadrupolar parameters for each of the five oxygen environments in coesite are correlated with the Si−O−Si bridging bond angles determined by diffraction experiments. The sign of e^2qQ/h along with the orientation of the electric field gradient for oxygen in the Si−O−Si linkage were determined from a Townes−Dailey analysis of the data.

1. Introduction

The recent application of ^{17}O dynamic-angle spinning[1−4] (DAS) nuclear magnetic resonance (NMR) spectroscopy to both crystalline and amorphous silicates has provided a considerable amount of new information concerning the short- and medium-range structures around oxygen in these materials.[5−7] One type of information is in the form of ^{17}O quadrupolar coupling parameters, which are a measure of the electric field gradient (efg) tensor at the oxygen nucleus. Knowledge of the efg tensor can be related to the local distribution of electrons and the arrangement of charge on neighboring atoms or ions, thus providing insight into the character of the chemical bonds and the bonding wave functions. In general, the calculation of the efg tensor at a particular nucleus in a solid requires knowledge of the ground-state electronic wavefunction and all atomic positions. While a full *ab initio* calculation can be problematic in solids, it has been shown that small clusters modeling silicate tetrahedral linkage can be effective models for bonding in solid silicates.[8,9] Indeed, ^{17}O efg tensors calculated using *ab initio* methods in a number of small clusters exhibit trends that correlate well with experimentally measured efg tensors in solid silicates.[10−13] Another approach that is less exact but has the advantage of providing analytical expressions for correlating efg tensors to structure is the Townes−Dailey model[14] for calculating efg tensors. This approach was first applied to ^{17}O efg tensor data measured by NMR in borates and silicates by Bray and co-workers[15,16] and in a number of zeolites and related materials by Oldfield and co-workers.[17,18] Unfortunately, the lack of a large database of ^{17}O quadrupolar coupling parameters made it difficult to further refine the application of *ab initio* or the Townes−Dailey approaches to ^{17}O efg tensor calculations in silicates. The recent advent of DAS, however, has considerably improved this situation.

In this paper we present solid-state ^{17}O NMR results on the silica polymorph coesite. Coesite is an ideal solid for confirming the correlations between the measured ^{17}O quadrupolar coupling parameters and the oxygen environment. From diffraction studies[19−21] coesite is known to have five distinct oxygen sites in a ratio of 1:1:2:2:2, with Si−O−Si bridging bond angles of 180.00°, 142.56°, 144.46°, 149.53°, and 137.22°, respectively. This set of bridging bond angles provides a good range over which to check the correlations between Si−O−Si angle and ^{17}O quadrupolar parameters.

2. Experimental Procedures

2.1. Coesite Preparation and Characterization. ^{17}O-labeled coesite (SiO_2) was made by first reacting $SiCl_4$ with 40% ^{17}O-labeled H_2O. The products of SiO_2, HCl, and residual H_2O were then heated to 1000 °C to remove the HCl, H_2O, and any other impurities, leaving pure silica. This sample was welded into a Pt capsule with a small amount (1−3%) of H_2O (unenriched) to speed kinetics and then heated in a piston cylinder apparatus at 900 °C and 35 kbar to transform the SiO_2. Slow recrystallization at these elevated pressures over 24 h allowed for the formation of a nearly pure coesite phase sample. Attempts to add Fe_2O_3 impurities to act as an NMR relaxing agent were unsuccessful, and therefore, an undoped sample was prepared for the final experiments. The samples was character-

* To whom correspondence should be addressed.
† Present address: Centre de Recherches sur la Physique des Hautes Temperatures, 1D Ave de la Recherche Scientifique, 45071 Orleans CEDEX 2, France.
‡ Present address: Department of Chemistry, Indiana University, Bloomington, IN 47405.
® Abstract published in *Advance ACS Abstracts*, July 1, 1995.

0022-3654/95/2099-12341$09.00/0

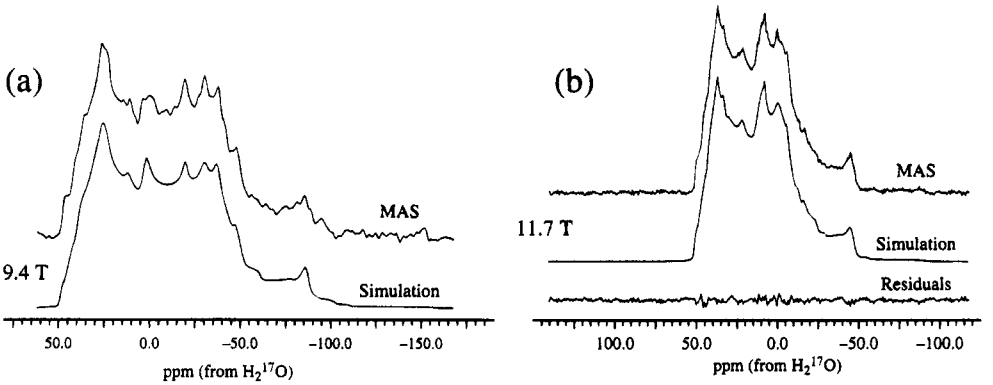

Figure 1. Magic-angle spinning (MAS) spectra and simulations of ^{17}O in coesite at (a) 9.4 T (54.544 MHz) and (b) 11.7 T (67.797 MHz). All spectra are referenced relative to ^{17}O-labeled H_2O. The simulation at 9.4 and 11.7 T were generated using the parameters in Table 1.

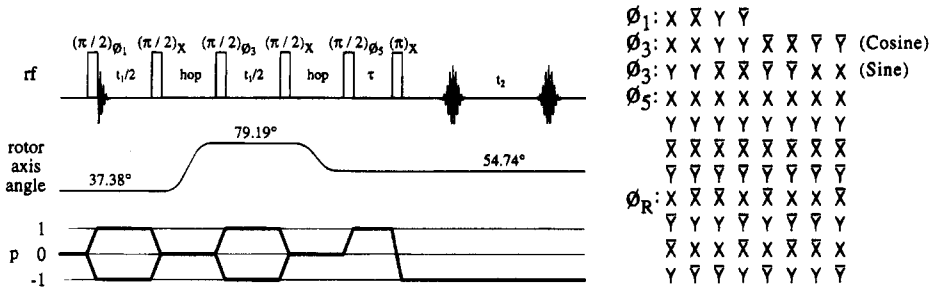

Figure 2. Pulse sequence, coherence transfer pathway, and minimal phase cycle for MAS-detected shifted-echo dynamic-angle spinning. ϕ_1, ϕ_3, and ϕ_5 are the rf phases of the pulses shown above, and ϕ_R is the receiver phase.

ized by both powder X-ray diffraction and ^{29}Si MAS NMR at 9.4 T. The powder X-ray diffraction pattern showed only a coesite phase with no significant impurities. The ^{29}Si MAS spectrum (not shown) agreed with previously published spectra[22] with peaks at -108.3 and -114.1 ± 0.1 ppm relative to external tetramethylsilane.

2.2. NMR Spectroscopy. All experiments at 11.7 T were performed on a Chemagnetics CMX500 spectrometer using a modified version of a home-built DAS probe described earlier.[23] All experiments at 9.4 T were performed on a Varian VXR400S spectrometer with a commercial (Doty Scientific, Inc.) 5 mm high-speed MAS probe. All experiments were done at ambient temperature with sample spinning rates between 13 and 15 kHz. The integrated intensities of the spinning sidebands were less than 12% of the total intensity at 11.7 T. The ^{17}O T_1 relaxation time of approximately 100 s for all sites was measured at 11.7 T for coesite using a saturation recovery experiment.

Bloch decay experiments were used to obtain the ^{29}Si MAS spectra. The Hahn echo sequence ($90-\tau-180-$acquire) was used to collect the ^{17}O MAS spectra at both 9.4 and 11.7 T. The recycle delays were set to 3600 and 1000 s, respectively. The ^{17}O MAS spectra are shown in Figure 1.

The DAS angle pair (37.38°, 79.19°) was employed in removing the second-order anisotropic broadenings, while detection was carried out at 54.74° to eliminate all chemical shift anisotropy contributions to the anisotropic line shapes.[24] The DAS pulse sequence employed is a modification of the hypercomplex shifted echo DAS sequence[25] and is shown in Figure 2. A DAS rotor reorientation time of 60 ms was used. To ensure selectivity of the ^{17}O central transition, $\pi/2$ times of 8.5 μs (at 37.38°), 7.5 μs (at 54.74°), and 6.5 μs (at 79.19°) were employed. The DAS echo was shifted by $\tau_{echo} = 1.5$ ms.[25] With a relaxation delay of 900 s between scans, 32 scans were averaged for each of the 47 × 256 hypercomplex $t_1 \times t_2$ points acquired. The dwell time in t_2 was 90.9 μs (11.1 kHz) and in t_1 was 100 μs (10 kHz). The t_1 dimension was zero-filled to 256 points, and no apodization was applied to t_1 dimension to try to retain the highest resolution possible; truncation artifacts ("sinc" wiggles) may be seen in the 2D DAS spectrum. The ^{17}O DAS spectrum is shown in Figure 3.

3. Results

3.1. NMR Data Reduction. For spin > 1/2 nuclei like ^{17}O, the quadrupolar coupling between its nuclear quadrupole moment and surrounding electric field gradient leads to an orientation dependence of its NMR transition frequency, which in a polycrystalline sample results in a characteristic line shape that can be analyzed to obtain the nuclear quadrupolar coupling parameters. In a static sample NMR experiment on a multisite system like coesite, these characteristic anisotropic NMR line shapes are overlapping, and therefore, the spectrum is not easily analyzed. Although MAS is designed to eliminate and effectively separate the anisotropic line shapes due to first-order perturbations like dipolar coupling and chemical shift, for ^{17}O the magnitude of quadrupolar coupling is often large enough that anisotropies due to second-order perturbations, which cannot be eliminated with MAS, are present. Therefore, ^{17}O MAS cannot completely eliminate and separate the anisotropic line shapes in coesite. However, with DAS both the first- and second-order orientation dependences are removed from the central $1/2 \rightarrow -1/2$ NMR transition of ^{17}O and the anisotropic NMR line shapes separated in a two-dimensional DAS spectrum.

The coesite MAS and DAS spectra were fit using a powder line shape simulation based on an algorithm described previously[26] and the CERN library MINUIT least-squares minimization subroutines. $\chi^2_{reduced}$ was determined using the noise in the baseline to estimate the error at each point in the spectrum. For all parameters we report larger uncertainties than those obtained from the first and second derivatives of $\chi^2_{reduced}$ at the minimum to account for the minor line shapes distortions due to finite spinning speeds, slight angle missettings, saturation effects, and other intensity distortions that are difficult to quantify.

The ^{17}O NMR parameters for the five oxygen sites in coesite obtained by fitting the DAS separated second-order quadrupolar

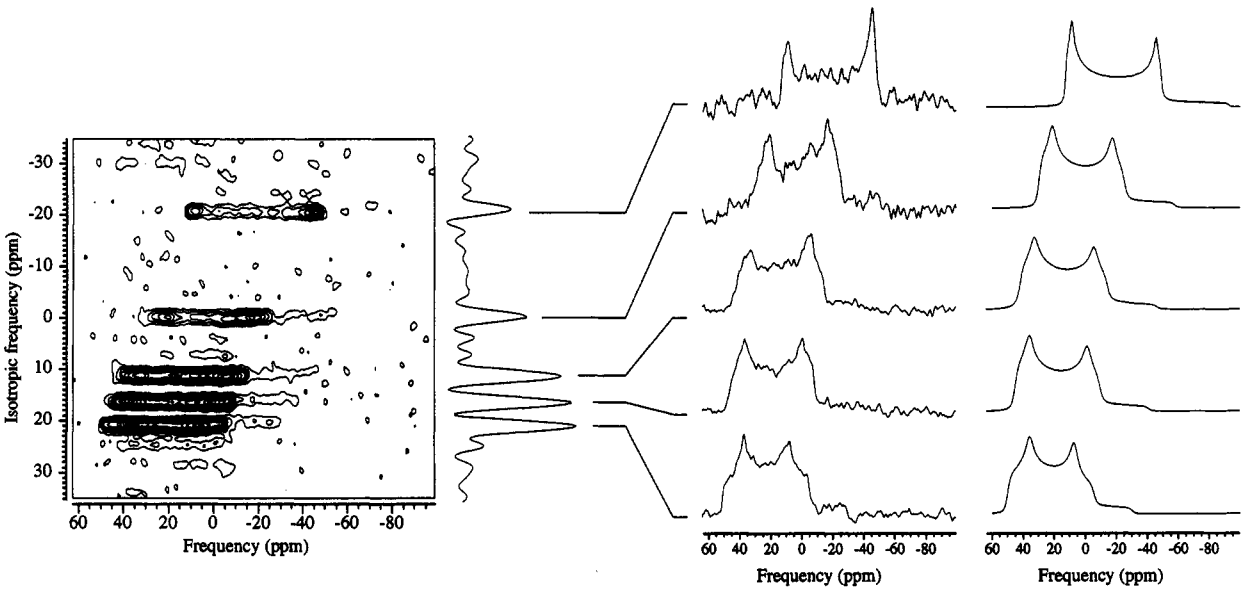

Figure 3. Two-dimensional DAS spectrum of ^{17}O in coesite at 11.7 T. The projection of the isotropic shift dimension is shown at the top. The contour lines are drawn at levels of 7, 16, 25, 34, 43, 52, 61, 71, 79, 88, and 97% of the maximum point in the spectrum. The spectrum is referenced relative to ^{17}O-labeled H_2O. Also shown are cross sections from the two-dimensional DAS spectrum taken parallel to the anisotropic (54.74°) dimension for the five sites in coesite. "Best-fit" simulations of the five sites are shown alongside each cross section. Best-fit quadrupolar and chemical shift parameters are listed in Table 1.

TABLE 1: Quadrupolar Coupling Parameters and Isotropic Chemical Shifts for the Five Oxygen Sites in Coesite Obtained from Least-Squares Fits of the 11.7 and 9.4 T MAS and 11.7 T DAS Spectra[a]

δ_{iso}^{obs} (ppm)	C_q (MHz)	η	δ_{iso}^{CS} (ppm)	intensity	assignment	∠Si−O−Si
−19.24 ± 2.00	6.05 ± 0.05	0.000 ± 0.005	29 ± 1	0.83 ± 0.1	O1	180.00°
1.54 ± 2.00	5.43 ± 0.05	0.166 ± 0.005	41 ± 1	1.05 ± 0.1	O2	142.56°
12.87 ± 2.00	5.52 ± 0.05	0.169 ± 0.005	53 ± 1	2.05 ± 0.1	O4	149.53°
17.92 ± 2.00	5.45 ± 0.05	0.168 ± 0.005	57 ± 1	2.16 ± 0.1	O3	144.46°
21.93 ± 2.00	5.16 ± 0.05	0.292 ± 0.005	58 ± 1	1.90 ± 0.1	O5	137.22°

[a] Because of the difficulties associated with external shift references, we report an uncertainty of ±2.00 in δ_{iso}^{obs}, however, relative shifts are accurate to within ±0.1 ppm. Minimum $\chi^2_{reduced}$ obtained was <5.

line shapes to single site line shapes and by fitting the 11.7 and 9.4 T MAS spectra to five overlapping second-order quadrupolar line shapes were in agreement within our experimental error and are listed in Table 1. The simulated anisotropic line shapes obtained with the parameters in Table 1 are shown along with the experimental MAS spectra in Figure 1 and along with the experimental DAS cross sections in Figure 3. While the signal-to-noise and least-squares fit are better for the MAS spectra than for the anisotropic DAS cross sections, without the DAS results it is difficult to justify that our MAS least-squares fit is the only unique fit for the MAS line shape.

It should be pointed out that to a small extent the quadrupolar asymmetry parameter η can be "exchanged" for Gaussian or Lorentzian line broadening without affecting the overall $\chi^2_{reduced}$ significantly. Therefore, the line broadening for each site was not allowed to vary in the least-squares fit and was held fixed at 30 Hz Lorentzian and 145 Hz Gaussian.

3.2. Assignments. Assignments of the five ^{17}O resonances to the five crystallographically distinct oxygens is based on the integrated intensities of the resonances and the empirical correlation[7] that the ^{17}O quadrupolar coupling constant, $C_q = e^2qQ/h$, increases with increasing Si−O−Si angle, while the ^{17}O quadrupolar coupling asymmetry parameter, η, decreases with increasing Si−O−Si angle. These correlations derive from both theoretical *ab initio* calculations on small clusters modeling silicate tetrahedral linkage[11,10] as well as experimental ^{17}O NMR results on other crystalline silicate systems.[27,28]

Detailed illustrations of the structure of coesite can be found in previous diffraction studies.[19−21] From these studies coesite is known to have five distinct oxygen sites in a ratio of 1:1:2:2:2 with Si−O−Si bridging bond angles of 180.00°, 142.56°, 144.46°, 149.53°, and 137.22°, respectively. This is in good agreement with the ratio of the integrated intensities for the five resonances in coesite. Therefore, the two low-intensity signals near 0 and −20 ppm must correspond to crystallographic sites O1 (180.00°) and O2 (142.56°). Of these two resonances the one near −20 ppm has the largest quadrupolar coupling constant and smallest asymmetry parameter and is therefore assigned to the O1 site. This means that the peak near 0 ppm must correspond to O2.

The other three crystallographic sites may be partially assigned by assuming that the site with the smallest bridging bond angle, O5 (137.22°), is assigned to the resonance near 22.3 ppm, which has the largest asymmetry parameter and smallest quadrupolar coupling constant. The remaining two sites, O4 (149.53°) and O3 (144.46°), must correspond to the two peaks near 13 and 18 ppm, respectively, based on their quadrupolar coupling parameters. The distinction between O4 and O3 is weaker since both the bond angles and the quadrupolar coupling parameters are very similar.

4. Analysis

We follow the Townes−Dailey model[14] as outlined by Bray and co-workers[15,16,29] and Oldfield and co-workers[17,18] for calculating the relationship between the efg of ^{17}O and angle in a Si−O−Si linkage. In this model the bonding and nonbonding valence electrons of oxygen in a Si−O−Si linkage

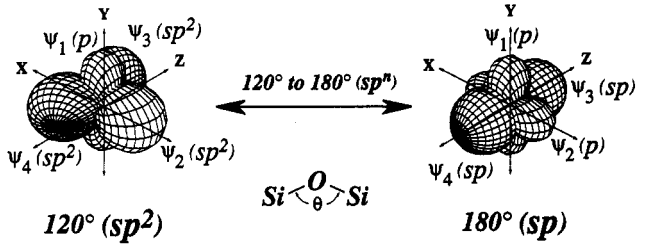

Figure 4. Schematic representation of the hybrid orbitals on oxygen in the Si−O−Si linkage.

TABLE 2: $\langle\phi_{nlm_l}|E_{2m}|\phi_{nlm'_l}\rangle$ **for** $l = 1$[a]

$$\langle\phi_{n1-1}|E_{2-2}|\phi_{n11}\rangle = -\sqrt{3/2}eq_{n1}$$
$$\langle\phi_{n10}|E_{2-1}|\phi_{n11}\rangle = -\sqrt{3/4}eq_{n1}$$
$$\langle\phi_{n1-1}|E_{2-1}|\phi_{n10}\rangle = \sqrt{3/4}eq_{n1}$$
$$\langle\phi_{n11}|E_{20}|\phi_{n11}\rangle = -eq_{n1}/2$$
$$\langle\phi_{n10}|E_{20}|\phi_{n10}\rangle = eq_{n1}$$
$$\langle\phi_{n1-1}|E_{20}|\phi_{n1-1}\rangle = -eq_{n1}/2$$
$$\langle\phi_{n11}|E_{21}|\phi_{n10}\rangle = \sqrt{3/4}eq_{n1}$$
$$\langle\phi_{n10}|E_{21}|\phi_{n1-1}\rangle = -\sqrt{3/4}eq_{n1}$$
$$\langle\phi_{n11}|E_{22}|\phi_{n1-1}\rangle = -\sqrt{3/2}eq_{n1}$$

[a] Matrix elements between Cartesian p orbitals are obtained using the definitions $|np_x\rangle = 1/\sqrt{2}[|\phi_{n1-1}\rangle - |\phi_{n11}\rangle]$, $|np_y\rangle = i/\sqrt{2}[|\phi_{n1-1}\rangle + |\phi_{n11}\rangle]$, and $|np_z\rangle = |\phi_{n10}\rangle$.

can be approximated to exist in four linear combination of atomic orbitals (LCAO approximation):

$$|\psi_1\rangle = |\phi_{2p_y}\rangle$$

$$|\psi_2\rangle = \gamma|\phi_{2s}\rangle + (1-\gamma^2)^{1/2}|\phi_{2p_x}\rangle$$

$$|\psi_3\rangle = \frac{1}{\sqrt{2}}\left[(1-\gamma^2)^{1/2}|\phi_{2s}\rangle - \gamma|\phi_{2p_x}\rangle + |\phi_{2p_z}\rangle\right] \quad (1)$$

$$|\psi_4\rangle = \frac{1}{\sqrt{2}}\left[(1-\gamma^2)^{1/2}|\phi_{2s}\rangle - \gamma|\phi_{2p_x}\rangle - |\phi_{2p_z}\rangle\right]$$

which form molecular orbitals (MO) with the atomic orbitals of silicon. Here $\gamma = \cot\theta/2$, where θ is the Si−O−Si bond angle. The fractional s character, f_s, of the sp^n ($1 \le n \le 2$) hybrid orbitals can be related to γ or θ according to

$$f_s(\theta) = \frac{1-\gamma^2}{2} = \frac{\cos\theta}{\cos\theta - 1} \quad (2)$$

$|\psi_2\rangle$, $|\psi_3\rangle$, and $|\psi_4\rangle$ are the sp^n hybrid orbitals. $|\psi_3\rangle$ and $|\psi_4\rangle$ form σ-bond MO's with silicon, while $|\psi_1\rangle$ and $|\psi_2\rangle$ may form π-bond MO's with the d orbitals of silicon.[30] A schematic representation of these orbitals is shown in Figure 4.

The efg that arises from n_k electrons ($0 \le n_k \le 2$) in the kth orbital is given by

$$\langle\psi_k|E_{2m}|\psi_k\rangle = n_k\sum_{i,j} a_i^* a_j\langle\phi_i|E_{2m}|\phi_j\rangle \quad (3)$$

where a_i are the orbital coefficients and the matrix elements $\langle\phi_i|E_{2m}|\phi_j\rangle$ are given in Table 2. The total efg that arises from all the bonding and nonbonding valence electrons is

$$\langle R_{2m}\rangle = \sum_k \langle\psi_k|E_{2m}|\psi_k\rangle \quad (4)$$

Other contributions to the efg can arise from the charges on surrounding atoms in the crystal lattice; however, as pointed out by Jellison et al.,[15] the lattice contribution can be ignored for the bridging oxygens, where the local contribution is an order of magnitude stronger.

Using the matrix elements in Table 2, we obtain

$$\langle R_{20}\rangle/eq_{21} = \frac{1}{2}\left[-n_1 - (1-\gamma^2)n_2 + \frac{2-\gamma^2}{2}(n_3+n_4)\right] \quad (5)$$

$$\langle R_{2\pm1}\rangle/eq_{21} = \sqrt{\frac{3}{8}}\gamma(n_4 - n_3) \quad (6)$$

$$\langle R_{2\pm2}\rangle/eq_{21} = \sqrt{\frac{3}{8}}\left[-n_1 + (1-\gamma^2)n_2 + \frac{\gamma^2}{2}(n_3+n_4)\right] \quad (7)$$

where eq_{21} is the ^{17}O quadrupolar coupling constant ($C_{q21} = e^2q_{21}Q/h = 20.88$ MHz) measured[31] in atomic oxygen due to one unbalanced p electron, including Sternheimer effects.[32]

For a symmetric linkage, such as Si−O−Si, we assume that $n_3 = n_4 = n_{34}$, and then $R_{2\pm1} = 0$ and the field gradient R_{2m} is diagonal. However, we cannot assume that the Z axis of the efg principal axis system (PAS) is the same as the MO z axis. Two other possibilities exist for the assignment of the efg PAS Z axis. One is obtained by a rotation of the tensor R_{2m} such that $x \rightarrow y$, $y \rightarrow z$, and $z \rightarrow x$. This transformation is represented as

$$R'_{20} = -\frac{1}{2}R_{20} + \sqrt{\frac{3}{2}}R_{2\pm2} \quad (8)$$

$$R'_{2\pm2} = -\sqrt{\frac{3}{8}}R_{20} - \frac{1}{2}R_{2\pm2} \quad (9)$$

The other possibility is a rotation that takes $x \rightarrow z$, $y \rightarrow x$, and $z \rightarrow y$. With this rotation we obtain

$$R''_{20} = -\frac{1}{2}R_{20} - \sqrt{\frac{3}{2}}R_{2\pm2} \quad (10)$$

$$R''_{2\pm2} = \sqrt{\frac{3}{8}}R_{20} - \frac{1}{2}R_{2\pm2} \quad (11)$$

Therefore, we consider three cases (recalling that in the efg PAS $C_q = eQ\langle R_{20}\rangle/h$ and $\eta C_q = \sqrt{6}eQ\langle R_{2\pm2}\rangle/h$).

(I) MO z axis is efg PAS Z axis:

$$C_q/C_{q21} = \frac{1}{2}(n_{34} - n_1) + (n_{34} - n_2)f_s(\theta) \quad (12)$$

$$\eta C_q/C_{q21} = \frac{3}{2}(c_{34} - n_1) - 3(n_{34} - n_2)f_s(\theta) \quad (13)$$

(II) MO y-axis is efg PAS Z axis:

$$C'_q/C_{q21} = \frac{1}{2}(n_{34} - n_1) - 2(n_{34} - n_2)f_s(\theta) \quad (14)$$

$$\eta' C'_q/C_{q21} = \frac{3}{2}(n_{34} - n_1) \quad (15)$$

(III) MO x-axis is efg PAS Z axis

$$C''_q/C_{q21} = -(n_{34} - n_1) + (n_{34} - n_2)f_s(\theta) \quad (16)$$

$$\eta'' C''_q/C_{q21} = 3(n_{34} - n_1)f_s(\theta) \quad (17)$$

We have two experimentally measured parameters, $|C_q|$ and $|\eta|$, and in each of the above cases we have three unknown

TABLE 3: Orbital Populations Differences Obtained from a Townes–Dailey Analysis of the ^{17}O Quadrupolar Coupling Parameters for the Five Oxygen Sites in Coesite[a]

		Case I: MO z is PAS z		Case II: MO y is PAS z		Case III: MO x is PAS z	
C_q (MHz)	η	$n_{34}-n_1$	$n_{34}-n_2$	$n_{34}-n_1$	$n_{34}-n_2$	$n_{34}-n_1$	$n_{34}-n_2$
			O1, $\theta_{Si-O-Si}=180°$				
6.05	0.000	0.290	0.290	0.000	−0.290	0.000	0.290
−6.05	0.000	−0.290	−0.290	0.000	0.290	0.000	−0.290
			O4, $\theta_{Si-O-Si}=149.53°$				
5.52	0.169	0.279	0.269	0.030	−0.269	−0.032	0.251
−5.52	0.169	−0.279	−0.269	−0.030	0.269	0.032	−0.251
5.52	−0.169	0.249	0.302	−0.030	−0.302	0.032	0.320
−5.52	−0.169	−0.249	−0.302	0.030	0.302	−0.032	−0.320
			O3, $\theta_{Si-O-Si}=144.46°$				
5.45	0.168	0.276	0.275	0.029	−0.275	−0.033	0.255
−5.45	0.168	−0.276	−0.275	−0.029	0.275	0.033	−0.255
5.45	−0.168	0.246	0.307	−0.029	−0.307	0.033	0.327
−5.45	−0.168	−0.246	−0.307	0.029	0.307	−0.033	−0.327
			O2, $\theta_{Si-O-Si}=142.56°$				
5.43	0.166	0.274	0.278	0.029	−0.278	−0.033	0.257
−5.43	0.166	−0.274	−0.278	−0.029	0.278	0.033	−0.257
5.43	−0.166	0.246	0.310	−0.029	−0.310	0.033	0.331
−5.43	−0.166	−0.246	−0.310	0.029	0.310	−0.033	−0.331
			O5, $\theta_{Si-O-Si}=137.22°$				
5.16	0.292	0.271	0.264	0.048	−0.264	−0.057	0.225
−5.16	0.292	−0.271	−0.264	−0.048	0.264	0.057	−0.225
5.16	−0.292	0.223	0.320	−0.048	−0.320	0.057	0.359
−5.16	−0.292	−0.223	−0.320	0.048	0.320	−0.057	−0.359

[a] Three different cases are considered for the orientation of the efg along with both signs of the quadrupolar coupling constant and asymmetry parameter. Changing the sign of the asymmetry parameter is equivalent to exchanging the x and y axes of the efg PAS.

parameters (n_1, n_2, n_{34}). By making an assumption about the charge on the oxygen, we can solve for all three parameters; however, as an intermediate step we will solve for the differences $n_{34}-n_1$ and $n_{34}-n_2$ which can be obtained from just $|C_q|$ and $|\eta|$ alone.

(I) MO z axis is efg PAS Z axis:

$$n_{34}-n_1 = C_q/C_{q21}\frac{\eta+3}{3} \tag{18}$$

$$n_{34}-n_2 = -C_q/C_{q21}\frac{\eta-3}{6f_s(\theta)} \tag{19}$$

(II) MO y axis is efg PAS Z axis:

$$n_{34}-n_1 = C_q/C_{q21}\frac{2\eta}{3} \tag{20}$$

$$n_{34}-n_2 = C_q/C_{q21}\frac{\eta-3}{6f_s(\theta)} \tag{21}$$

(III) MO x axis is efg PAS Z axis:

$$n_{34}-n_1 = -C_q/C_{q21}\frac{2\eta}{6f_s(\theta)} \tag{22}$$

$$n_{34}-n_2 = -C_q/C_{q21}\frac{2\eta-6f_s(\theta)}{12f_s^2(\theta)} \tag{23}$$

In Table 3 are the population differences obtained for the five oxygen sites in coesite. For each of the 3 cases there are 2 possibilities for the sign of C_q and 2 possibilities for the sign of η, giving us a total of 12 sets of possible population differences for each site. Changing the sign of η is equivalent to exchanging the X and Y axes of the efg PAS.

TABLE 4: Average Orbital Populations Differences Obtained from a Townes–Dailey Analysis of the ^{17}O Quadrupolar Coupling Parameters for the Five Oxygen Sites in Coesite

		Case I: MO z is PAS z		Case II: MO y is PAS z		Case III: MO x is PAS z	
C_q	η	$n_{34}-n_1$	$n_{34}-n_2$	$n_{34}-n_1$	$n_{34}-n_2$	$n_{34}-n_1$	$n_{34}-n_2$
+	+	0.278	0.275	0.027	−0.275	−0.031	0.256
−	+	−0.278	−0.275	−0.027	0.275	0.031	−0.256
+	−	0.251	0.306	−0.027	−0.306	0.031	0.325
−	−	−0.251	−0.306	0.027	0.306	−0.031	−0.325

It is commonly assumed that the Si–O bond is approximately 50% ionic (i.e., $n_{34} \approx 1.5$).[33] Therefore, any population differences in Table 3 that are positive would imply that n_1 or n_2 (i.e., the "lone pair" populations) would have populations less than n_{34} (i.e., the "bonding pair" populations). This seems unreasonable even if π-bonding to the d orbitals of silicon exists. Therefore, we eliminate those efg orientations and signs with positive population differences. For case I this leaves only a negative efg; the magnitude of both $n_{34}-n_1$ and $n_{34}-n_2$ would imply a weak π-bonding to the silicon d orbitals that becomes weaker at smaller Si–O–Si angles. For case II only a positive efg and negative η remain, while in case III only a negative efg and negative η remain. For both cases II and III $n_{34}-n_1$ is near zero for all angles, implying strong π-bonding of the oxygen p orbital to the silicon d orbitals at all angles, and $n_{34}-n_2$ varies from −0.290 at 180° to −0.359 at 137.22°, implying a weaker π-bonding of the oxygen hybrid orbital to the silicon d orbitals that becomes weaker at smaller Si–O–Si angles.

From eqs 12–17 is it clear that both C_q/C_{q21} and $\eta C_q/C_{q21}$ will vary linearly as a function of $f_s(\theta)$, with slopes and intercepts that are proportional to the population differences $n_{34}-n_1$ and $n_{34}-n_2$. Ignoring for now the slight dependence of the population differences on the Si–O–Si angle, we can use the average population differences (see Table 4) in eqs 12–17 to determine which of the three cases for the efg PAS orientation best matches the measured quadrupolar parameters of coesite.

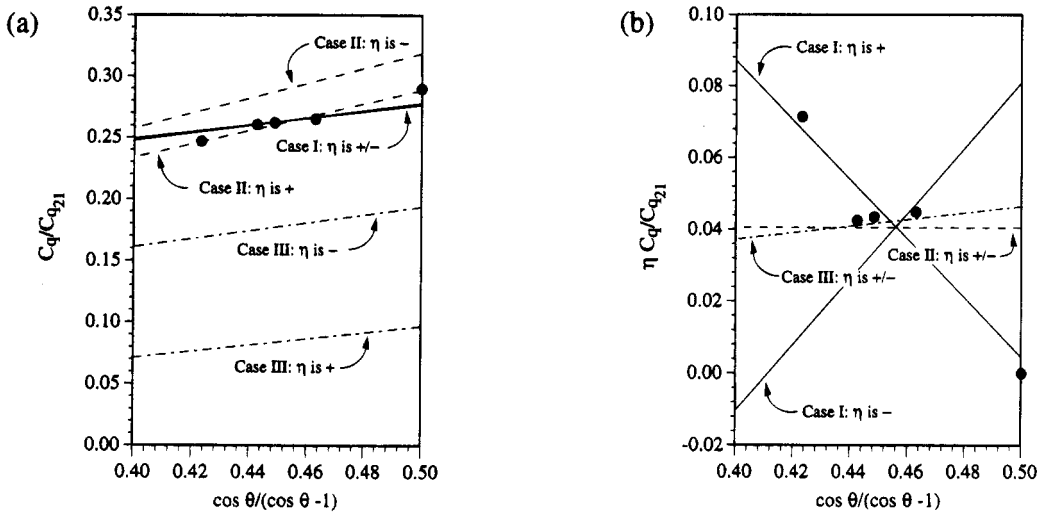

Figure 5. Plots of (a) C_q/C_{q21} and (b) $\eta C_q/C_{q21}$ vs fractional s character of the hybrid sp^n orbitals. Experimental data are represented by the symbol ●. Solid and dashed lines represent the variations of C_q/C_{q21} and $\eta C_q/C_{q21}$ expected for the three possible orientations of the efg PAS when using the average orbital population differences in Table 4.

TABLE 5: Orbital Populations Obtained from a Townes–Dailey Analysis of the ^{17}O Quadrupolar Coupling Parameters for the Five Oxygen Sites in Coesite, Assuming the x and z Axes of the Oxygen efg PAS Lie in the Plane of the Si–O–Si Bond with the x Axis Bisecting the Si–O–Si Bond Angle[a]

	O1, $\theta_{Si-O-Si} = 180°$, $C_q = -6.05$ MHz, $\eta = 0.000$			O4, $\theta_{Si-O-Si} = 149.53°$, $C_q = -5.52$ MHz, $\eta = 0.169$			O3, $\theta_{Si-O-Si} = 144.46°$, $C_q = -5.45$ MHz, $\eta = 0.168$			O2, $\theta_{Si-O-Si} = 142.56°$, $C_q = -5.43$ MHz, $\eta = 0.166$			O5, $\theta_{Si-O-Si} = 137.22°$, $C_q = -5.16$ MHz, $\eta = 0.292$		
Q	n_1	n_2	n_{34}	n_1	n_2	n_{34}	n_1	n_2	n_{34}	n_1	n_2	n_{34}	n_1	n_2	n_{34}
−0.50	1.770	1.770	1.480	1.767	1.757	1.488	1.763	1.762	1.487	1.762	1.765	1.487	1.763	1.755	1.491
−0.75	1.832	1.832	1.543	1.830	1.820	1.550	1.826	1.825	1.550	1.824	1.827	1.549	1.825	1.817	1.554
−1.00	1.895	1.895	1.605	1.892	1.882	1.613	1.888	1.890	1.612	1.887	1.890	1.612	1.888	1.880	1.616

[a] Populations are calculated for three different charges, Q, on oxygen.

In Figure 5a is a plot of C_q vs $f_s(\theta)$ for the five oxygen sites in coesite. From this plot is clear that case III, where the z axis of the efg PAS coincides with the MO x axis, can be eliminated. In Figure 5b is a plot of ηC_q vs $f_s(\theta)$. From this plot it is clear that in addition to case III, case II can also be eliminated along with case I where η is negative. This leaves only case I where η is positive for the orientation of the ^{17}O efg in the Si–O–Si linkage. Thus, we conclude that the ^{17}O efg in the Si–O–Si linkage is negative and has a PAS that coincides with the MO axis system described in eq 1. This is in agreement with that predicted by Janes and Oldfield.[17]

By defining the charge on the oxygen atom, Q, according to

$$Q = 6 - (n_1 + n_2 + 2n_{34}) \tag{24}$$

we can solve for all three populations:

$$n_1 = \frac{1}{4}C_q/C_{q21}\left[n + 3 + \frac{\eta - 3}{6f_s(\theta)}\right] - Q/4 + 3/2$$

$$n_2 = \frac{1}{4}C_q/C_{q21}\left[-\frac{\eta + 3}{3} - \frac{\eta - 3}{2f_s(\theta)}\right] - Q/4 + 3/2 \tag{25}$$

$$n_{34} = \frac{1}{4}C_q/C_{q21}\left[-\frac{\eta + 3}{3} + \frac{\eta - 3}{6f_s(\theta)}\right] - Q/4 + 3/2$$

Stewart and Spackman reported pseudoatom oxygen charges of -0.514 ± 0.048 obtained from the X-ray charge density map of low quartz.[34] Newton and Gibbs[8] calculated a charge of -0.65 esu for oxygen in a SiO_2 moiety of the low quartz structure in an STO-3G* *ab initio* MO calculation that included the 3d AO's of Si. We will assume charges of -0.5, -0.75, and -1 esu for oxygen to obtain the complete Townes–Dailey orbital population analysis of the ^{17}O quadrupolar coupling parameters for the five oxygen sites in coesite presented in Table 5.

That both n_1 and n_2 are less than 2 suggests that d–p π-bonding exists between the silicon d orbitals and the lone pair electrons on oxygen. In order to increase both n_1 and n_2 to a value of 2 in the Townes–Dailey analysis, it would be necessary to increase the charge Q. As can be seen in Table 5, increasing the charge leads to unrealistic values for n_{34} (i.e., making the Si–O bond > 50% ionic) before n_1 and n_2 reach 2. Therefore, our analysis supports a model where d–p bonding exists; however, since n_1 and n_2 do not appear to vary significantly as a function of angle, the d–p π-bonding is not structurally significant[35] and is more consistent with the constant overlap model as described by Janes and Oldfield,[17] as predicted by the *ab initio* calculations of Lindsay and Tossell.[10]

5. Discussion

Given the sign and orientation of the efg obtained from the above analysis of the coesite data, it appears that n_1 and n_2 are approximately equal and a simpler form can be obtained for the correlation between C_q and the Si–O–Si angle

$$C_q = C_{q21}(n_{34} - n_{12})\left(\frac{1}{2} + f_s(\theta)\right) = C_{q21}(n_{34} - n_{12})\left(\frac{1}{2} + \frac{\cos\theta}{\cos\theta - 1}\right) \tag{26}$$

and between η and the Si–O–Si angle

$$\eta = 6\frac{1 + 2f_s(\theta)}{1 - 2f_s(\theta)} = -\frac{3(\cos\theta + 1)}{3\cos\theta - 1} \tag{27}$$

where $n_{12} = n_1 = n_2$.

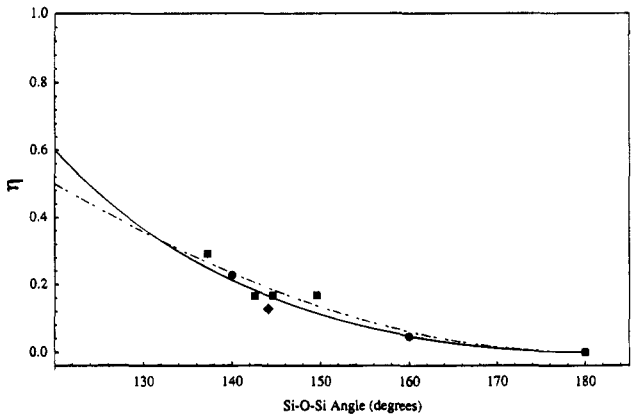

Figure 6. Plot of η vs Si−O−Si angle. Experimental ^{17}O data for coesite and cristobalite are represented by the symbols ■ and ◆, respectively, and the *ab initio* ^{17}O data for cluster $H_3Si-O-SiH_3$[11] are represented by the symbol ●. The solid line represents eq 27 and dot-dashed line represents eq 28.

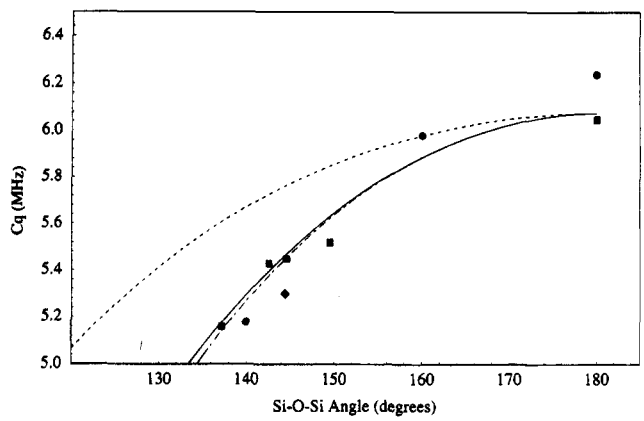

Figure 7. Plot of C_q vs Si−O−Si angle. Experimental ^{17}O data for coesite and cristobalite are represented by the symbols ■ and ◆, respectively, and the *ab initio* ^{17}O data for cluster $H_3Si-O-SiH_3$[10] are represented by the symbol ●. The dashed line represents eq 26 with $n_{34} - n_{12}$ held at a constant value of 0.29 and $C_{q21} = 20.88$ MHz. The solid line represents eq 31 with a $\Delta n_0 = 0.29$ and $C_{q21} = 20.88$ MHz. The dot-dashed line represents eq 32 with $C_q(180°) = 6.06$ MHz.

The expression for η, which is independent of orbital populations, was derived earlier by Sternberg[36] assuming only σ-bonding in the Si−O−Si linkage. This expression remains valid even if d−p π-bonding exists as long as $n_1 = n_2$ and $n_3 = n_4$ (i.e., eq 27 may not apply for ^{17}O in an asymmetric linkage, e.g., Al−O−Si, where $n_3 \neq n_4$ or $n_1 \neq n_2$). A plot of ^{17}O efg asymmetry parameters vs Si−O−Si angle for the coesite data as well as other data is presented in Figure 6. Included on the plot is the curve of eq 27 as well as the curve of the *ab initio* based empirical correlation,[11]

$$\eta = 1 + \cos\theta \tag{28}$$

which we had used previously[7] in an ^{17}O DAS study of $K_2Si_4O_9$ glass. Although both curves are in reasonable agreement with the experimental data, significant deviations between eqs 27 and 28 occur at angles near 120°, where no experimental data have yet been obtained.

Although the expression for η (eq 27) is independent of orbital populations, the expression for C_q depends linearly on $n_{34} - n_{12}$. From the coesite data it is apparent that $n_{34} - n_{12}$ is slightly dependent on the Si−O−Si angle. This behavior is also found in our Townes−Dailey analysis of the quadrupolar parameters obtained in the *ab initio* calculations of Tossell and co-workers.[11,10] This angle dependence is not accounted for in the Townes−Dailey molecular orbital analysis and can arise from a number of different possibilities. One possibility, that as the Si−O−Si angle widens to 180° there is an increase in the π overlap between the silicon d orbitals and the oxygen "lone pair" sp hybrid orbital (i.e. $|\psi_2\rangle$) while the π overlap between the silicon d orbitals and the oxygen "lone pair" p orbital (i.e. $|\psi_1\rangle$) remains constant, can be ruled out since both orbital differences $n_{34} - n_1$ and $n_{34} - n_2$ vary to the same degree with angle. One explanation that is consistent with the observed increase of orbital population differences with Si−O−Si angle could be that as the Si−O−Si angle widens, the Si−O σ bonds become more ionic (i.e., the charge on oxygen increases), while the π overlap between the silicon d orbitals and both oxygen "lone pair" orbitals remains constant. However, another explanation could be that the orbital population differences are constant while C_{q21} varies with angle. It has been suggested that C_{q21} is slightly charge dependent,[37]

$$C_{q21}^{\text{eff}} = C_{q21}(1.2)^{Q} \tag{29}$$

and therefore, C_{q21}^{eff} would also increase with Si−O−Si angle. There certainly could be a combination of effects, along with other possibilities. Thus, although analytical expressions describing the MO dependence on Si−O−Si angle exist, analytical expressions for trends in orbital populations or charge with Si−O−Si are not as easily derived. Therefore, additional assumptions are necessary to obtain a more quantitative fit of the Townes−Dailey model to the experimental data. To this end, we simply introduce the empirical correlation

$$\Delta n = \Delta n_0\left(\frac{1}{2} + \frac{\cos\theta}{\cos\theta - 1}\right) \tag{30}$$

where $\Delta n = n_{34} - n_{12}$ and $\Delta n_0 = 0.29$ for the Si−O−Si linkage. With this expression we obtain

$$C_q = C_{q21}\Delta n_0\left(\frac{1}{2} + \frac{\cos\theta}{\cos\theta - 1}\right)^2 \tag{31}$$

Previously,[7] we had assumed a simple dependence of C_q on the variation of the oxygen fractional s character with Si−O−Si angle given by

$$C_q = C_q(180°)\frac{2\cos\theta}{\cos\theta - 1} \tag{32}$$

where $C_q(180°)$ is equivalent to $C_{q21}\Delta n_0$. A plot of ^{17}O quadrupolar coupling constants vs Si−O−Si angle for the coesite data as well as other data is presented in Figure 7. Included on the plot are the curves of eq 26 with $n_{34} - n_{12}$ held constant and eqs 31 and 32. Although the curve of eq 26 has the correct trend of C_q with Si−O−Si angle, a more quantitative agreement is obtained with the curves of eqs 31 and 32. In general, the Townes−Dailey derived expressions for η (eq 27) and C_q (eq 31) have the advantage of being more directly connected to the MO picture of the Si−O−Si linkage.

Finally, it is interesting to note that on the basis of the *ab initio* calculations of Tossell and co-workers[10,11] for the cluster $H_3Si-O-SiH_3$, one might predict for coesite a monotonic variation of the ^{17}O isotropic chemical shift with Si−O−Si angle over a range of <10 ppm. The observed variation in coesite (see Table 1), however, is not monotonic with Si−O−Si angle and varies over a much wider range of 29 ppm. In fact, this variation constitutes a significant fraction of the total range of shifts measured to date for ^{17}O in crystalline silicates.[27] Thus, although the efg for the five inequivalent oxygens in coesite can be described, to a good approximation, solely in terms of their Si−O−Si angle, this doesn't appear to be the case for the

chemical shift tensor. Obviously, other factors are involved. One possible clue seen in the detailed crystal structure drawings of refs 38 and 20 may be that the sites which have chemical shifts of 57, 53, and 58 ppm, i.e., sites O3, O4, and O5, respectively, are part of four rings which are linked together to form a double crankshaft chain along the (101) axis. In contrast the sites which have the lower chemical shifts of 29 and 41 ppm, i.e., sites O1 and O2, respectively, cross-link these double crankshaft chains and are part of 6- and 8-ring structures. Although it has been observed that ^{29}Si chemical shifts in siloxane ring oligomers are strongly correlated to ring size,[39,40] little is known concerning ring size effects on ^{17}O chemical shifts in similar compounds. Clearly, more ^{17}O NMR investigations of crystalline silicates will be needed before these issues are fully resolved.

6. Conclusions

Using ^{17}O dynamic-angle spinning and magic-angle spinning, we have resolved and assigned all five oxygen sites in coesite, a silica polymorph. We have obtained the quadrupolar coupling parameters for all sites from anisotropic line shape analysis and have found that a correlation between Si−O−Si angle and ^{17}O quadrupolar parameters supports previous theoretical as well as experimental correlations.

A Townes−Dailey analysis of the data indicates that the sign of the oxygen efg is negative and that the x and z axes of the oxygen efg PAS lie in the plane of the Si−O−Si bond with the x axis bisecting the Si−O−Si bond angle. This is in agreement with the orientation predicted by Janes and Oldfield.[17] A Townes−Dailey orbital population analysis suggests that d−p π-bonding exists between the lone pair valence electrons of oxygen and the d orbitals of silicon but is not structurally significant.

These data and their analysis should prove helpful in making the correlation between the isotropic ^{17}O NMR line shapes and quadrupolar coupling data obtained from 2D DAS spectra of silicate glasses and their medium-range structural order.[7,41]

Acknowledgment. The high-pressure synthesis was performed by Steve R. Bohlen at the USGS facility at Menlo Park, CA. P.J.G. acknowledges helpful discussions with Pierre Florian and Jim Downs. This work was supported by the Director of the Office of Energy Research, Office of Basic Energy Sciences, Materials Sciences Division of the U.S. Department of Energy under Contract No. DE-AC03-76SF00098 and by the National Science Foundation, through Grant No. EAR-9204458 to J.F.S. J.H.B. was supported by a NSF graduate fellowship and a Camille and Henry Dreyfus start-up grant. U.W. thanks the Alexander von Humboldt Foundation for a Feodor Lynen Fellowship.

References and Notes

(1) Samoson, A.; Lippmaa, E.; Pines, A. *Mol. Phys.* **1988**, *65*, 1013.
(2) Chmelka, B. F.; Mueller, K. T.; Pines, A.; Stebbins, J.; Wu, Y.; Zwanziger, J. W. *Nature* **1989**, *339*, 42.
(3) Llor, A.; Virlet, J. *Chem. Phys. Lett.* **1988**, *152*, 248.
(4) Grandinetti, P. J. Dynamic-Angle Spinning and Applications. In *Encyclopedia of Nuclear Magnetic Resonance*; Grant, David M., Harris, Robin K., Eds.; John Wiley & Sons: New York, 1995.
(5) Mueller, K. T.; Wu, Y.; Chmelka, B. F.; Stebbins, J.; Pines, A. *J. Am. Chem. Soc.* **1991**, *113*, 32.
(6) Mueller, K. T.; Baltisberger, J. H.; Wooten, E. W.; Pines, A. *J. Phys. Chem.* **1992**, *96*, 7001.
(7) Farnan, I.; Grandinetti, P. J.; Baltisberger, J. H.; Stebbins, J. F.; Werner, U.; Eastman, M. A.; Pines, A. *Nature* **1992**, *358*, 31.
(8) Newton, M. D.; Gibbs, G. V. *Phys. Chem. Miner.* **1980**, *6*, 221.
(9) Gibbs, G. V. *Am. Mineral* **1982**, *67*, 421.
(10) Lindsay, C. G.; Tossell, J. A. *Phys. Chem. Miner.* **1991**, *18*, 191.
(11) Tossell, J. A.; Lazzeretti, P. *Phys. Chem. Miner.* **1988**, *15*, 564.
(12) Tossell, J. A.; Lazzeretti, P. *Chem. Phys. Lett.* **1987**, *112*, 205.
(13) Tossell, J. A. *J. Non-Cryst. Solids* **1990**, *120*, 13.
(14) Townes, C. H.; Dailey, B. P. *J. Chem. Phys.* **1949**, *17*, 782.
(15) Jellison, G. E.; Panek, L. W.; Bray, P. J.; Rouse, G. B. *J. Chem. Phys.* **1977**, *66*, 802.
(16) Geissberger, A. E.; Bray, P. J. *J. Non-Cryst. Solids* **1983**, *54*, 121.
(17) Janes, N.; Oldfield, E. *J. Am. Chem. Soc.* **1986**, *108*, 5743.
(18) Timken, H. K. C.; Janes, N.; Turner, G. L.; Lambert, S. L.; Welsh, L. B.; Oldfield, E. *J. Am. Chem. Soc.* **1986**, *108*, 7236.
(19) Gibbs, G. V.; Prewitt, C. T.; Baldwin, K. J. *Z. Kristallogr.* **1977**, *145*, 108.
(20) Smyth, J. R.; Smith, J. V.; Artioli, G.; Kvick, A. *J. Phys. Chem.* **1987**, *91*, 988.
(21) Geisinger, K. L.; Spackman, M. A.; Gibbs, G. V. *J. Phys. Chem.* **1987**, *91*, 3237.
(22) Smith, J. V.; Blackwell, C. S. *Nature* **1983**, *303*, 223.
(23) Eastman, M. A.; Grandinetti, P. J.; Lee, Y. K.; Pines, A. *J. Magn. Reson.* **1992**, *98*, 333.
(24) Mueller, K. T.; Wooten, E. W.; Pines, A. *J. Magn. Reson.* **1990**, *92*, 620.
(25) Grandinetti, P. J.; Baltisberger, J. H.; Llor, A.; Lee, Y. K.; Werner, U.; Eastman, M. A.; Pines, A. *J. Magn. Reson. Ser.* **1993**, *103*, 72.
(26) Alderman, D. W.; Solum, M. S.; Grant, D. M. *J. Chem. Phys.* **1986**, *84*, 3717.
(27) Stebbins, J. F. Nuclear Magnetic Resonance Spectroscopy of Silicates and Oxides in Geochemistry and Geophysics. In *Handbook of Physical Constants*; American Geophysical Union: Washington DC, 1994.
(28) Xue, X.; Stebbins, J. F.; Kanzaki, M. *Am. Mineral* **1994**, *79*, 31.
(29) Schempp, E.; Bray, P. J. Nuclear Quadrupolar Resonance Spectroscopy. In *Physical Chemistry, An Advanced Treatise*; Henderson, D., Ed.; Academic Press: New York, 1970.
(30) Cruickshank, D. W. J. *J. Chem. Soc.* **1961**, *1077*, 5486.
(31) Harvey, J. S. M. *Proc. R. Soc. London, Ser. A* **1965**, *285*, 581.
(32) Sternheimer, R. M. *Phys. Rev.* **1950**, *80*, 102.
(33) Pauling, L. *The Nature of the Chemical Bond*; Cornell University Press: Ithaca, NY, 1960.
(34) Stewart, R. F.; Spackman, M. A. Charge Density Distributions. In *Structure and Bonding in Crystals*; O'Keefe, Navrotsky, Eds.; Academic Press: New York, 1981; Vol. 1, p 279.
(35) Cruickshank, D. W. J. *J. Mol. Struct.* **1985**, *130*, 177.
(36) Sternberg, U. *Solid State Nucl. Magn. Reson.* **1993**, *2*, 181.
(37) Lucken, E. A. C. *Nuclear Quadrupolar Coupling Constants*; Academic Press: New York, 1969.
(38) Levien, L.; Prewitt, C. T. *Am. Mineral.* **1981**, *66*, 324.
(39) Tossell, J. A. *Chem. Mater.* **1994**, *6*, 239.
(40) Harsmann, H. ^{17}O and ^{29}Si NMR. In *NMR Basic Principles and Progress*; Diehl, Fluck, Kosfeld, Eds.; Springer-Verlag: Berlin, 1981; Vol. 17.
(41) Grandinetti, P. J.; Baltisberger, J. H.; Werner, U.; Pines, I.; Farnan, I.; Stebbins, J. F. In preparation.

JP950094C